On the application and interpretation of Keeling plots in paleo climate research ? deciphering ?13C of atmospheric CO2 measured in ice cores

P. Köhler, H. Fischer, J. Schmitt, G. Munhoven

Biogeosciences, 3, 539–556, 2006
www.biogeosciences.net/3/539/2006/

Biogeosciences

On the application and interpretation of Keeling plots in paleo climate research – deciphering $\delta^{13}C$ of atmospheric CO_2 measured in ice cores

P. Köhler[1], H. Fischer[1], J. Schmitt[1], and G. Munhoven[2]

[1]Alfred Wegener Institute, Helmholtz Center for Polar and Marine Research, P.O. Box 12 01 61, 27515 Bremerhaven, Germany
[2]Laboratoire de Physique Atmosphérique et Planétaire, Institut d'Astrophysique et de Géophysique, Université de Liège, 17 avenue du Six-Août, B–4000 Liège, Belgium

Received: 21 February 2006 – Published in Biogeosciences Discuss.: 14 June 2006
Revised: 9 November 2006 – Accepted: 10 November 2006 – Published: 15 November 2006

Abstract. The Keeling plot analysis is an interpretation method widely used in terrestrial carbon cycle research to quantify exchange processes of carbon between terrestrial reservoirs and the atmosphere. Here, we analyse measured data sets and artificial time series of the partial pressure of atmospheric carbon dioxide (pCO_2) and of $\delta^{13}C$ of CO_2 over industrial and glacial/interglacial time scales and investigate to what extent the Keeling plot methodology can be applied to longer time scales. The artificial time series are simulation results of the global carbon cycle box model BICYCLE. The signals recorded in ice cores caused by abrupt terrestrial carbon uptake or release loose information due to air mixing in the firn before bubble enclosure and limited sampling frequency. Carbon uptake by the ocean cannot longer be neglected for less abrupt changes as occurring during glacial cycles. We introduce an equation for the calculation of long-term changes in the isotopic signature of atmospheric CO_2 caused by an injection of terrestrial carbon to the atmosphere, in which the ocean is introduced as third reservoir. This is a paleo extension of the two reservoir mass balance equations of the Keeling plot approach. It gives an explanation for the bias between the isotopic signature of the terrestrial release and the signature deduced with the Keeling plot approach for long-term processes, in which the oceanic reservoir cannot be neglected. These deduced isotopic signatures are similar ($-8.6‰$) for steady state analyses of long-term changes in the terrestrial and marine biosphere which both perturb the atmospheric carbon reservoir. They are more positive than the $\delta^{13}C$ signals of the sources, e.g. the terrestrial carbon pools themselves ($\sim -25‰$). A distinction of specific processes acting on the global carbon cycle from the Keeling plot approach is not straightforward. In general, processes related to biogenic fixation or release of carbon have lower y-intercepts in the Keeling plot than changes in physical processes, however in many case they are indistinguishable (e.g. ocean circulation from biogenic carbon fixation).

1 Introduction

In carbon cycle research information on the origin of fluxes between different reservoirs as contained in the ratio of the stable carbon isotopes $^{13}C/^{12}C$ has become more and more important in the past decades. Differences in physical properties of atoms and molecules containing different isotopes of an element lead to isotopic fractionation during most physico-chemical processes. Isotopic ratios therefore store information about ongoing or past processes.

Prominent examples of processes during which isotopic fractionation occurs in our context of global carbon cycle research are gas exchange between surface ocean and atmosphere or photosynthetic production in both the marine and the terrestrial biosphere. Here, the carbon reservoir which includes the end members of a carbon flux associated with a given process is in general depleted in the heavier isotope. This is expressed with the fractionation ε of the process, which depends on various environmental parameters such as temperature or the biological species (see Zeebe and Wolf-Gladrow (2001) for more basic information on carbon isotopes in seawater).

Correspondence to: P. Köhler
(pkoehler@awi-bremerhaven.de)

Published by Copernicus GmbH on behalf of the European Geosciences Union.

The isotopic composition of a reservoir is usually expressed in per mil (‰) in the so-called "δ-notation" as the relative deviation from the isotope ratio of a defined standard (VPDP in the case of $\delta^{13}C$):

$$\delta^{13}C_{\text{ sample}} = \left(\frac{\frac{^{13}C}{^{12}C\,\text{sample}}}{\frac{^{13}C}{^{12}C\,\text{standard}}} - 1 \right) \times 10^3. \quad (1)$$

The fractionation ε (in ‰) between carbon in sample A and in sample B (e.g. before and after some fractionation step) is related to the δ values by

$$\varepsilon_{(A-B)} = \frac{\delta^A - \delta^B}{1 + \delta^B/10^3}. \quad (2)$$

During photosynthesis the carbon taken up by marine primary producers is typically depleted by -16 to -20‰. On land, the type of metabolism determines the fractionation during terrestrial photosynthesis. C_3 plants exhibit a higher discrimination against the heavy isotope (ε=-15 to -23‰) than plants with C_4 metabolism (ε=-2 to -8‰) (Mook, 1986).

One prominent interpretation technique of carbon exchange between the atmosphere and other reservoirs, e.g. used in carbon flux studies in terrestrial ecosystems, is plotting the $\delta^{13}C$ signature of CO_2 as a function of the inverse of the atmospheric carbon dioxide mixing ratio ($\delta^{13}C = f(1/CO_2)$). In doing so, the intercept of a linear regression with the y-axis can under certain conditions be understood as the isotopic signature of the flux, which alters the content of carbon in the atmospheric reservoir. This approach is called "Keeling plot" after the very first usage by Charles D. Keeling about 50 years ago (Keeling, 1958, 1961). Keeling plots are widely used for data interpretation in terrestrial carbon research, however, their application is based on some fundamental assumptions (see review of Pataki et al., 2003).

Keeling plots have also been used in paleo climate research in the past years (e.g. Smith et al., 1999; Fischer et al., 2003). However, one of the fundamental limitations of the Keeling plot approach, which is its restriction to fast exchange processes, has not been taken into account adequately in these studies. Therefore, the aim of this paper is to emphasise what can be learnt from Keeling plots, if applied on slow, but global processes acting on glacial/interglacial time scales, and to discuss their limitations. We emphasise what kind of information can be gained from deciphering the $\delta^{13}C$ signal measured in ice cores. For this purpose we first extent the Keeling plot approach to a three reservoir system and then analyse measured data sets and artificial time series, the latter produced by a global carbon cycle box model. The advantage of the analysis of model output is, that we know which processes were active and thus responsible for the changes in the global carbon cycle.

2 The original Keeling plot

The Keeling plot approach is based upon mass conservation considerations during the exchange of carbon between two reservoirs. Let C_{new} be the mass of carbon after the addition of carbon with mass C_{add} to an reservoir with an initial mass C_{old}.

$$C_{new} = C_{old} + C_{add} \quad (3)$$

We denote by $\delta^{13}C_x$ the carbon isotopic signature of the C component x, conservation of mass requires that

$$C_{new}\delta^{13}C_{new} = C_{old} \cdot \delta^{13}C_{old} + C_{add} \cdot \delta^{13}C_{add}. \quad (4)$$

By combining Eqs. (3) and (4) we obtain a relationship between $\delta^{13}C_{new}$ and C_{new}:

$$\delta^{13}C_{new} = (\delta^{13}C_{old} - \delta^{13}C_{add})\frac{C_{old}}{C_{new}} + \delta^{13}C_{add}. \quad (5)$$

Thus, the y-intercept y_0 of the linear regression function of Eq. (5), which describes $\delta^{13}C_{new}$ as a function of the inverse of the carbon content ($1/C_{new}$), gives us the isotopic signature $\delta^{13}C_{add}$ of the carbon added to the reservoir.

There are two basic assumptions underlying the Keeling plot method: (1) The system consists of only two reservoirs. (2) The isotopic ratio of the carbon in the added reservoir does not change during the time of observation. Both assumptions are only rarely fulfilled. Furthermore, there are arguments about which linear regression model should be used if one assumes measurement errors in both variables (for details see Pataki et al., 2003). The methodological aspects concerning the choice of a regression model are not the subject of our investigations here.

The Keeling plot approach was used in the past to interpret various different sub-systems of the global carbon cycle. Keeling (1958, 1961) first used it to identify the contribution of terrestrial plants to the background isotopic ratio of CO_2 in a rural area near the Pacific coast of North America. Later, the contribution of the terrestrial biosphere in the seasonal cycle of CO_2 over Switzerland (Friedli et al., 1986; Sturm et al., 2005) and Eurasia (Levin et al., 2002) was investigated with the Keeling plot. The approach was widely used in terrestrial ecosystem research to identify respiration fluxes (e.g. Flanagan and Ehleringer, 1998; Yakir and Sternberg, 2000; Bowling et al., 2001; Pataki et al., 2003; Hemming et al., 2005). It was used in paleo climate research within the last years to disentangle the processes explaining the subtle changes in CO_2 during the relatively stable Last Glacial Maximum (LGM) and the Holocene as well as the approximately 80 ppmv increase from the LGM to the Early Holocene (Smith et al., 1999; Fischer et al., 2003).

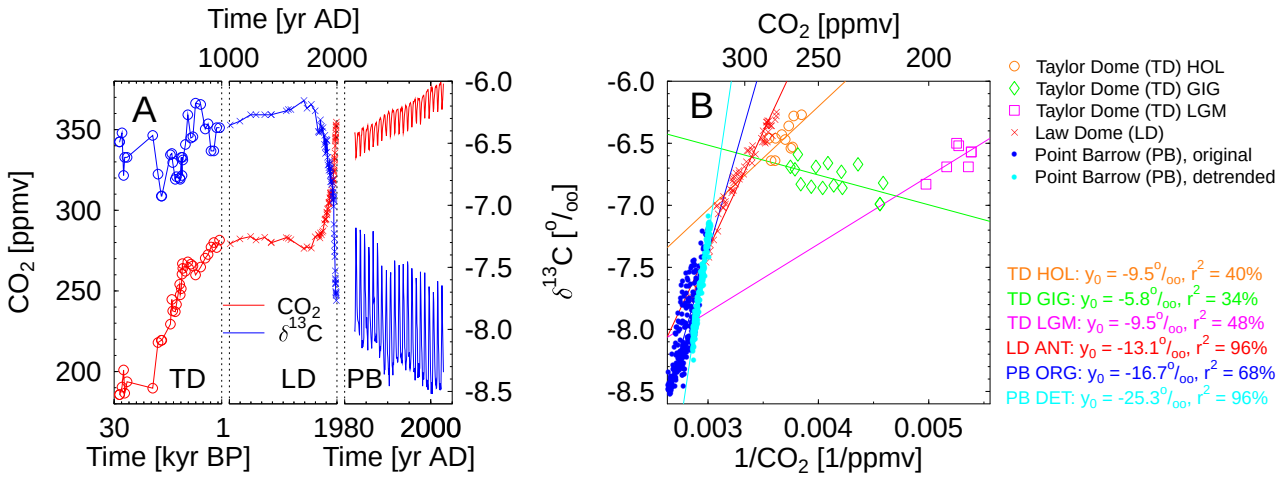

Fig. 1. A compilation of data from Point Barrow (PB), the Law Dome (LD), and the Taylor Dome (TD) ice cores (**(a)**: CO_2, $\delta^{13}C$; **(b)**: Keeling plot). Monthly resolved data (1982−2002) from Point Barrow (Keeling and Whorf, 2005; Keeling et al., 2005). Only times where data in both CO_2 and $\delta^{13}C$ were available are considered here. For the Keeling plot approach the original data (PB ORG) and detrended time series (PB DET) are plotted and analysed. Data from firn and ice at Law Dome cover the last millenium (Francey et al., 1999; Trudinger et al., 1999) which includes the anthropogenic rise in CO_2 (LD ANT). Data from the Taylor Dome ice core of the last 30 kyr include the glacial/interglacial transition during Termination I (Smith et al., 1999) with the age model of Brook et al. (2000). Taylor Dome data are split into the Holocene (TD HOL), the glacial/interglacial transition (TD GIG), and the LGM (TD LGM).

3 Global CO_2 and $\delta^{13}C$ time series of different temporal resolution

Fischer et al. (2003) used Keeling plots to analyse the seasonal amplitudes of CO_2 and $\delta^{13}C$ during the past few decades, the anthropogenic rise in CO_2 and the concomitant $\delta^{13}C$ decrease since 1750 AD, as well as their glacial/interglacial variations. As illustrated in Fig. 1, these three data sets which cover three completely different temporal scales exhibit significantly different behaviour.

As an example we take the seasonality of the atmospheric carbon records at Point Barrow, Alaska, covering the period from 1982 to 2002 AD (Keeling and Whorf, 2005; Keeling et al., 2005) where the seasonal cycle in CO_2 and $\delta^{13}C$ is most pronounced. For the interpretation of this data set, the time series need to be detrended to separate the seasonality from the simultaneously occurring anthropogenic long-term trend. Annual variations are then analysed as perturbations from the mean values of the first year of the measurements.

For the anthropogenic variation during the last millennium we use the data measured in air enclosures in the Law Dome ice core (Francey et al., 1999; Trudinger et al., 1999). The component C_{add} in Eqs. (3)–(5) reflects the exchange of carbon of an external reservoir with the atmospheric reservoir. The Point Barrow and Law Dome data can be approximated consistently with the typical Keeling plot linear regression function (r^2=96% in both). The y-axis intercept y_0 increases from the seasonal effects (−25‰) to the anthropogenic impact (−13‰) with the mixed signal of the undetrended data at Point Barrow in-between (−17‰) (Fig. 1b). This increase is explained by a larger oceanic carbon uptake and a smaller airborne fraction of any atmospheric disturbance in CO_2 in the longer time series from the Law Dome ice core (Fischer et al., 2003).

These two examples based on measured data sets are already beyond the scope of Keeling's original idea as they are no longer based on a two reservoir system and highlight the limitations of this approach. While the y-intercept of the detrended data at Point Barrow is consistent with the expected value, the intercept found in the anthropogenic rise in Law Dome does not record the $\delta^{13}C$ signal of the carbon released by anthropogenic activity to the atmosphere. The seasonal amplitude at Point Barrow can be explained with the seasonality of the terrestrial biosphere. Vegetation grows mainly in the northern hemisphere, and thus CO_2 minima occur during maximum photosynthetic carbon uptake by plants during northern summer. The seasonal fluctuation in CO_2 should therefore bear a $\delta^{13}C$ signal of the order of −25‰ which would account for fractionation during terrestrial photosynthesis (Scholze et al., 2003). This $\delta^{13}C$ signal of the seasonal cycle is seen in the detrended Point Barrow data in agreement with other studies (e.g. Levin et al., 2002). The rise seen in the Law Dome data set is the result of the combination of anthropogenic activities (fossil fuel emissions (Marland et al., 2005) and land use changes (Houghton, 2003), Fig. 2), terrestrial carbon sinks due to CO_2 fertilisation (Plattner et al., 2002), all from which the ocean carbon uptake during that time has to be subtracted. Without carbon uptake by the ocean and the terrestrial reservoirs this would have led to a rise in atmospheric CO_2 by more than 200 ppmv.

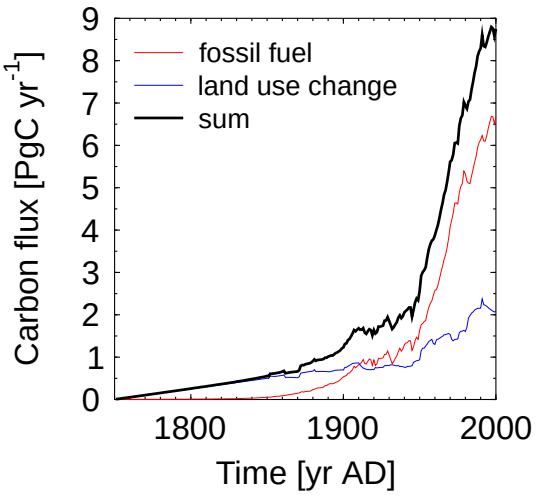

Fig. 2. Annual fluxes of fossil fuel emissions since 1750 AD (Marland et al., 2005), and land use change since 1850 AD (Houghton, 2003), the later linearly extrapolated to zero in year 1750 AD.

The $\delta^{13}C$ signal of recent fossil fuel emissions in the USA is around -29 to -30‰ (Blasing et al., 2004), while carbon fluxes from land use changes bear the typical $\delta^{13}C$ signal of the terrestrial biosphere (-25‰). These isotopic signatures of anthropogenic processes are by no means reflected in the Keeling plot analysis. The reason for this is that due to the gas exchange between ocean and atmosphere the basic assumption of a two reservoir system is intrinsically violated. This questions the applicability of the Keeling plot approach to carbon change studies on long time scales, where this ocean/atmosphere gas exchange becomes even more significant.

Going further back in time, the glacial/interglacial rise in CO_2 and its concomitant $\delta^{13}C$ variations as measured in the Taylor Dome ice core ($1-30$ kyr BP) led to a sub-grouping of the $\delta^{13}C$–$1/CO_2$ data pairs (Smith et al., 1999) with different linear regression functions for the Last Glacial Maximum (LGM), the glacial/interglacial transition (GIG), and the Holocene (HOL) (Fig. 1b). With on average one data point every thousand years the data set is sparse. The y-intercepts for the LGM and the Holocene subsets are similar (-9.5‰) and significantly different from that during the transition (-5.8‰). Thus, it was hypothesised that underlying processes for variations in CO_2 during the relatively stable climates of the LGM and the Holocene might have been the same and might have been mainly based on processes concerning the terrestrial biosphere (Smith et al., 1999; Fischer et al., 2003). The even higher y-intercepts of carbon dynamics during the glacial/interglacial transition (GIG) compared to those of the anthropogenic era (Fig. 1b) have been explained by the longer time scale of those changes in the Holocene and the LGM, allowing for equilibration of the ocean/atmosphere carbon reservoirs.

4 Extending the Keeling plot approach to a three reservoir system

A first-order estimate of the carbon isotopic signature in the atmosphere due to a slow injection of terrestrial carbon into the ocean/atmosphere system can be derived when extending the original system to a three reservoir system. Here we assume that ocean circulation remains unchanged during the injection and that an equilibrium between ocean and atmosphere is achieved. This extension is adjusting the first assumption of the original Keeling plot approach (two reservoir system), which restricts potential applications to fast processes where the effect of gas exchange between ocean and atmosphere can be neglected. In this extended three reservoir system the steady states prior to and after a perturbation are compared and thus the long-term component of an experiment is envisaged. We will develop an equation which calculates the changes in the isotopic signature of atmospheric CO_2 caused by these long-term changes and call this the *effective isotopic signature* or $\delta^{\Delta A}$ of the underlying process, which here is the injection of terrestrial carbon. For fast processes (two reservoir system only), the effective isotopic signature $\delta^{\Delta A}$ is identical with $\delta^{13}C_{add}$, the signature of the carbon added to the atmosphere. It is the direct analogue of the y-intercept of the linear regression model in the classical Keeling plot. For processes that are not fast enough the effect of gas exchange and equilibration between ocean and atmosphere is not negligible. Therefore, this y-intercept of a linear regression model through the $1/CO_2$-$\delta^{13}C$-diagram will no longer accurately record the isotopic signature of the perturbation. The theoretical developments reported below will show what information this y-intercept bears in case the fundamental two reservoir only assumption of the original Keeling plot is not fulfilled. We hence propose a new interpretation methodology and process understanding which extends the range of applicability of the original Keeling plot approach.

In the three reservoir system under consideration, the mass balance equations are

$$A + O = A_0 + O_0 + B \tag{6}$$

and

$$A\delta^A + O\delta^O = A_0\delta_0^A + O_0\delta_0^O + B\delta^B. \tag{7}$$

These are equivalents of the Eqs. (3) and (4) in the two reservoir system. In these two equations, A_0 and O_0 represent the amounts of carbon in the atmosphere and the ocean, respectively, prior to the perturbation by the injection of an amount B of biospheric carbon while A and O are the amounts after the injection; δ_0^A and δ_0^O are the ^{13}C isotopic characteristics of the atmospheric and oceanic carbon reservoirs before, δ^A and δ^O those after the injection and δ^B is that of the biospheric carbon. Typical values for a pre-industrial initial state are A_0=600 PgC, O_0=38 000 PgC

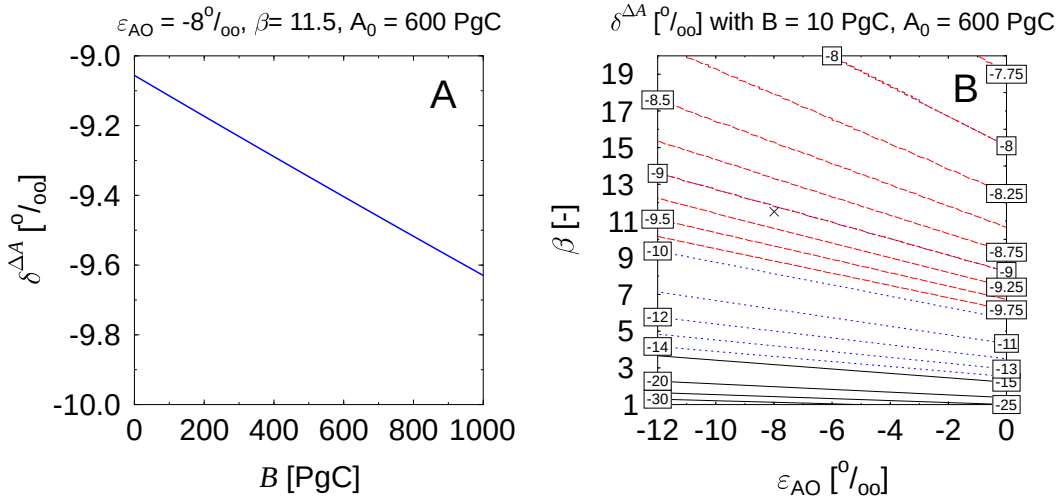

Fig. 3. Results of the extended Keeling approach with three reservoirs. Effective isotopic signature of the atmosphere $\delta^{\Delta A}$ as function of **(a)** the size of the terrestrial release and **(b)** the Revelle Factor β and the fractionation during gas exchange ε_{AO}. Other variables as given in the figures. The cross in panel (b) marks the preindustrial state (β= 11.5, ε_{AO}=−8.0‰). Contour lines for $\delta^{\Delta A}$ in panel (b) have three equidistances: 5‰ (black, solid), 1‰ (blue, short broken), 0.25‰ (red, long broken).

with δ_0^A=−6.5‰ and δ_0^O=+1.5‰. For the terrestrial biospheric carbon, a typical value of δ^B=−25‰ is adopted. During air-sea gas exchange and carbonic acid dissociation in seawater fractionation occurs (according to Eq. (2)): $\varepsilon_{AO} \approx \delta_0^A - \delta_0^O \approx \delta^A - \delta^O \approx -8‰$, which is assumed to remain constant in time.

For the oceanic uptake of carbon the buffering effect of the carbonate system in seawater needs to be taken into account (Zeebe and Wolf-Gladrow, 2001). The ratio between the change in CO_2 concentration and the change in dissolved inorganic carbon (DIC) is described by the Revelle or buffer factor β, which depends on temperature, alkalinity and DIC:

$$\beta = \left(\frac{d\mathrm{CO_2}/\mathrm{CO_2}}{d\mathrm{DIC}/\mathrm{DIC}} \right). \tag{8}$$

Any additional carbon injected into the ocean/atmosphere system will be distributed between the two reservoirs according to the ratio of the sizes before the injection, i.e.

$$\frac{A - A_0}{O - O_0} = \beta \frac{A_0}{O_0}. \tag{9}$$

The Revelle factor β in modern surface waters varies between 8 and 16 (Sabine et al., 2004). For the preindustrial setting β in the surface ocean boxes of our box model BICYCLE is on average 11.5, with 9 in equatorial waters and around 12 at high latitude. The average Revelle factor of the LGM surface ocean is close to 10 due to the higher carbon uptake in waters with colder temperature. The buffering effect of the carbonate system was thus smaller at the LGM than at preindustrial times.

The effective isotopic signature $\delta^{\Delta A}$ of the perturbation in the atmosphere can be estimated according to

$$\delta^{\Delta A} = \frac{A\delta^A - A_0\delta_0^A}{A - A_0}. \tag{10}$$

Starting from the Eq. (10), the expression for $\delta^{\Delta A}$ can be rewritten so that it is only a function of the initial values A_0, O_0, δ_0^A and δ_0^O, the perturbation B, δ^B and the parameters β and ε_{AO}:

$$\delta^{\Delta A} = \delta_0^A + \left(\delta^B - \delta_0^A + \frac{\varepsilon_{AO}}{\beta \frac{A_0}{O_0} + 1} \right) \frac{A_0 + \frac{O_0}{\beta} + B}{A_0 + O_0 + B}. \tag{11}$$

The pathway from Eq. (10) to Eq. (11) is detailed in Appendix A.

It is obvious from Eq. (11) that for the special case where β=1 (no carbonate buffering) and ε_{AO}=0‰ (no isotopic fractionation during air/sea transfer), $\delta^{\Delta A}$ is equal to the isotopic signature δ^B of the terrestrial carbon release. In this special case, the three reservoir system actually behaves like a two reservoir one and the original Keeling plot setting is recovered. In all other cases, both the buffering of the ocean and the isotopic fractionation during gas exchange have a significant influence on the calculated $\delta^{\Delta A}$.

A simple scale analysis of the different terms in Eq. (11) provides an order-of-magnitude estimate for the $\delta^{\Delta A}$ values that we may expect to observe. The two factors of the second term of the right hand side of the equation determine by how much $\delta^{\Delta A}$ differs from the initial isotopic signature of the atmosphere (δ_0^A). Using typical values of −8‰ for ε_{AO} and 10 for β, and further noticing that $A_0 \ll O_0$, we see that the term in brackets is dominated by δ^B. Since $B \ll O_0$ as well,

the multiplying factor $(A_0+\frac{O_0}{\beta}+B)/(A_0+O_0+B)$ is of the order of $1/\beta$. As a consequence $\delta^{\Delta A}$ will, in general, deviate by about δ^B/β or about $-2.5‰$ from δ_0^A.

Indeed, when we insert the values for isotopic signatures and reservoir sizes given above and vary the amount of terrestrial carbon added, the isotopic fractionation during gas exchange ε_{AO} or the Revelle factor β we obtain varying effective isotopic signatures $\delta^{\Delta A}$ of the change in the atmospheric carbon reservoir as shown in Fig. 3. In a typically preindustrial setting, $\delta^{\Delta A}$ varies nearly linearly with B between $-9‰$ and $-10‰$ (Fig. 3a), reflecting the progressive lightening of the overall ocean/atmosphere system when more isotopically depleted terrestrial carbon is added. These values are similar to those of Smith et al. (1999) and Fischer et al. (2003) both for the Holocene and the LGM from Taylor Dome ice core data, which have been interpreted as indicative of terrestrial carbon reservoir changes during these periods. However, from the interpretation of other processes changing the global carbon cycle following in Sect. 5.3 it will become apparent that there are other processes than the release of terrestrial carbon that can produce this kind of signal.

There are thus already three preliminary conclusions to be drawn:

1. The effective isotopic signature $\delta^{\Delta A}$ is dependent on the amount of carbon injected and the setting of the system described by the three reservoirs, their isotopic signatures, the fractionation factors, and the Revelle factor.

2. For realistic settings an injection of terrestrial carbon into the atmosphere/ocean produces a $\delta^{\Delta A}$ between -8.5 and $-10‰$. The calculated effective isotopic signature is therefore much more enriched in ^{13}C than the carbon released from the terrestrial biosphere with $\delta^B=-25‰$. This bias between expectation (δ^B) and calculation ($\delta^{\Delta A}$) is caused by the influence of the ocean and depends only on the system settings described in the previous conclusion.

3. There exists a limiting value $\delta^{\Delta A}_{\delta B\to 0}$ in the effective signature of the isotopic change in atmospheric δ^{13}C which is reached if the amount of carbon released to the atmosphere converges to zero.

Only for processes that are faster than the equilibration time of the deep ocean with the atmosphere, substantial amounts of isotopically depleted carbon stay in the atmosphere allowing for more negative effective $\delta^{\Delta A}$values in the Keeling plot. The latter is seen e.g. for the seasonal variation in CO_2 due to the waxing and waning of the biosphere and, to a smaller extent, also for the input of isotopically depleted anthropogenic carbon into the atmosphere which operates at typical time scales of decades to centuries.

The effective carbon isotopic signature $\delta^{\Delta A}$ based on our theoretical consideration as calculated in this section is comparable with the y_0 of a linear regression in a Keeling plot performed on measured or simulated data sets. This becomes obvious when equation (10) is used to express δ^A as a function of $1/A$:

$$\delta^A = (\delta_0^A - \delta^{\Delta A})\frac{A_0}{A} + \delta^{\Delta A}, \tag{12}$$

which is identical to Eq. (5). However, this comparison is, strictly speaking, only valid if the perturbation in the carbon cycle is of terrestrial origin. Details in the marine carbon cycle, such as spatial variations in the Revelle factor, ocean circulation schemes and the ocean carbon pumps which introduce vertical gradients in DIC and ^{13}C in the ocean are not included in this analytical approach. This limitation prevents us to apply our theoretical framework directly to discriminate between processes of marine origin. Nevertheless, we will use the linear regression model in the $1/CO_2$-δ^{13}C-diagram of artificial time series, which were caused by long-term processes of marine and terrestrial origin to empirically analyse how far these processes can be distinguished by this method.

5 Artificial pCO_2 and δ^{13}C times series

Recently, a time-dependent modelling approach gave a quantitative interpretation of the dynamics of the atmospheric carbon records over Termination I by forcing the global ocean/atmosphere/biosphere carbon cycle box model BICYCLE forward in time (Köhler et al., 2005a). The authors identified the impacts of different processes acting on the carbon cycle on glacial/interglacial time scales and proposed a scenario, which provides an explanation for the evolution of CO_2, δ^{13}C, and Δ^{14}C over time. The results are in line with various other paleo climatic observations.

In the following we will reanalyse the results of Köhler et al. (2005a) by applying the Keeling plot analysis to study whether this kind of analysis applied on paleo climatic changes in atmospheric CO_2 and δ^{13}C can lead to meaningful results. Additional simulations with BICYCLE will be performed. The advantage of using model-generated artificial time series is, that we know which processes are operating and which process-dependent isotopic fractionations influence the δ^{13}C signals of the results. We highlight how the Keeling plot approach can gain new insights from these data sets and figure out its limitations in paleo climatic research.

Since BICYCLE does not resolve seasonal phenomena we are unable to interpret or, e.g., reconstruct the dynamics of the Point Barrow data set of the past few decades. However, we are able to implement the anthropogenic impacts of the last 250 years as seen in the Law Dome ice core.

5.1 The global carbon cycle box model BICYCLE

The box model of the global carbon cycle BICYCLE consists of an ocean module with ten homogeneous boxes in three basins (Atlantic, Southern Ocean, Indo-Pacific) and three different vertical layers (surface, intermediate, deep), a glob-

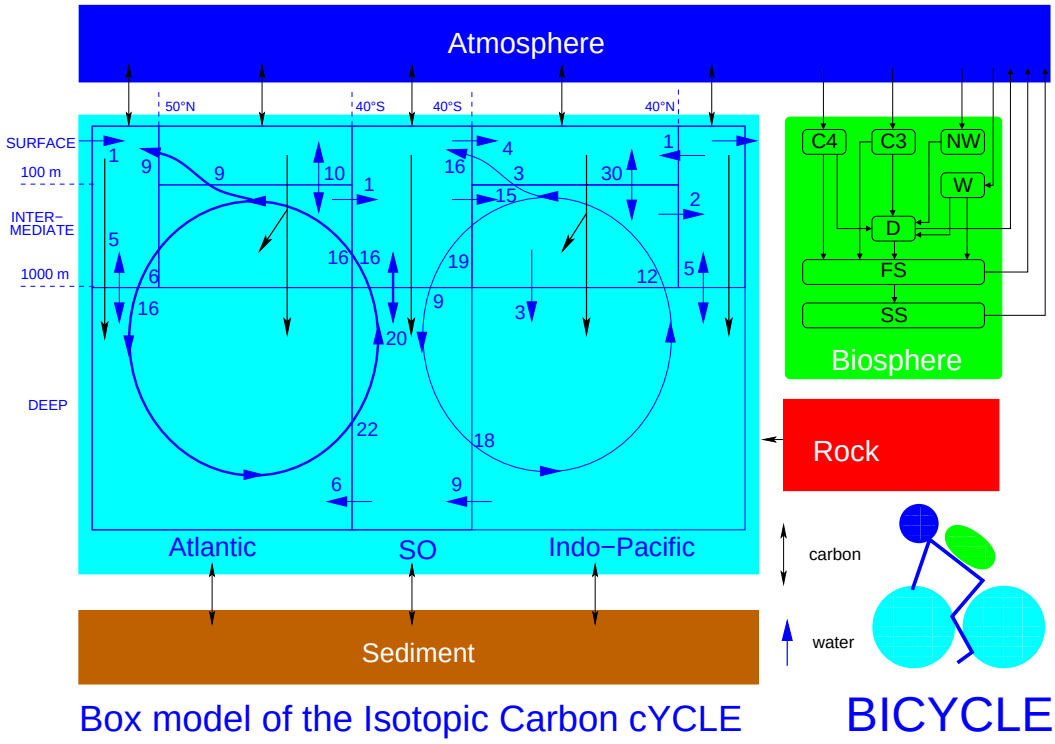

Fig. 4. A sketch of the BICYCLE model including boundary conditions and preindustrial ocean circulation fluxes (in Sv=10^6 m^2 s^{-1}) in the ocean module redrawn from Köhler et al. (2006a). The globally averaged terrestrial biosphere distinguishes ground vegetation following different photosynthetic pathways (C4, C3), non-woody (NW), and woody (W) parts of trees, and soil compartments (D, FS, SS) with different turnover times.

ally averaged atmospheric box and a terrestrial module with seven globally averaged compartments representing ground and tree vegetation and soil carbon with different turnover times (Fig. 4). Prognostic variables in the model are DIC, alkalinity, oxygen, phosphate and the carbon isotopes ^{13}C and ^{14}C in the ocean boxes, and carbon and its carbon isotopes in the atmosphere and terrestrial reservoirs. The net difference between sedimentation and dissolution of $CaCO_3$ is calculated from variations of the lysocline and determines the exchange of DIC and alkalinity between deep ocean and sediment. The model is completely described in Köhler and Fischer (2004) and Köhler et al. (2005a). The architecture of BICYCLE is derived from previous box models (Emanuel et al., 1984; Munhoven, 1997). It was adapted to study questions of paleo climate research and uses up-to-date parameterisations.

We apply disturbances of the climate system through the use of forcing functions and paleo climatic records (e.g. changes in temperature, sea level, aeolian dust input in the Southern Ocean) and prescribe changes in ocean circulation over time based on other data- and model-based studies. BICYCLE can then be used to interpret the evolution of atmospheric CO_2, $\delta^{13}C$, and $\Delta^{14}C$ (Köhler et al., 2005a). It was further used to simulate variations of atmospheric CO_2 during the last eight glacial cycles (Wolff et al., 2005; Köhler and Fischer, 2006), and to analyse the implication of changes in the carbon cycle on atmospheric $\Delta^{14}C$ (Köhler et al., 2006a).

5.2 Anthropogenic emissions – ground truthing of the paleo Keeling plot approach

We implement a data-based estimate of the anthropogenic emission since 1750 AD in our model as shown in Fig. 2. BICYCLE calculates pCO_2 depending on the dynamics of the terrestrial biosphere. In the more realistic case of an active terrestrial biosphere, which considers an enhanced photosynthesis and thus carbon uptake through CO_2 fertilisation, pCO_2 in 2000 AD is calculated to 351 μatm (Fig. 5c). A scenario with passive terrestrial biosphere, i.e., a constant carbon storage over time, leads to 388 μatm in the same year (Fig. 5a). In the year 2000 AD the annual mean in the atmospheric CO_2 data at Point Barrow is 371 ppmv, which is approximately half way between the results of the two different simulation scenarios. The scenario with passive terrestrial biosphere is easier to interpret, since we only have to consider the anthropogenic carbon flux to the atmosphere and the effect of the oceanic sink. Both scenarios will be analysed in the following.

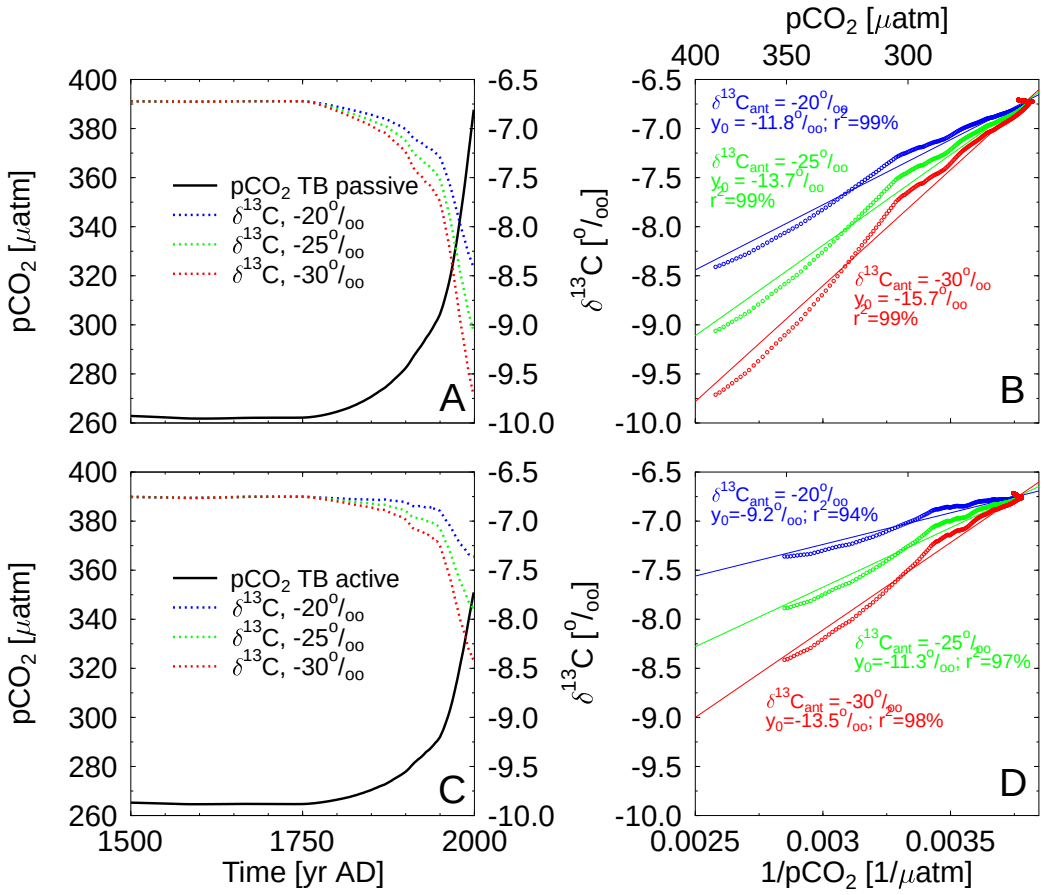

Fig. 5. Reconstructions of the rise in pCO_2 in the atmosphere during the last 500 years with BICYCLE (left: pCO_2, δ^{13}C; right: Keeling plot). Anthropogenic fluxes were used as plotted in Fig. 2. Two different settings are tested, one with passive terrestrial biosphere TB (top), meaning that carbon storage in the land reservoirs was kept constant, and one with active terrestrial biosphere (bottom), in which a rise in the internal calculated pCO_2 is enhancing terrestrial carbon uptake via its fertilisation effect. Different simulations with different isotopic signatures of the anthropogenic emission (−20‰, −25‰, −30‰).

The exact value of the δ^{13}C signature of anthropogenic carbon release is somewhat uncertain, e.g. land use change has a δ^{13}Cof −25‰ (Scholze et al., 2003), while δ^{13}C of fossil fuel emissions is around −30‰ (Blasing et al., 2004). We therefore adopted three different values of −20‰, −25‰, −30‰ for the anthropogenic carbon fluxes. The corresponding atmospheric δ^{13}C values in year 2000 AD were respectively −8.4‰, −9.1‰, −9.7‰ (passive biosphere) and −7.4‰, −7.9‰, −8.4‰ (active biosphere) reflecting a stronger terrestrial fixation of anthropogenic carbon when CO_2 fertilisation is considered (see Figs. 5a, c). The annual average δ^{13}C measured at different globally distributed stations varied between −8.0‰ and −8.2‰ (Keeling et al., 2005). Scenarios with an active terrestrial biosphere in combination with a δ^{13}C signature between −25‰ and −30‰ are thus most compatible with the observations.

The regression functions of the Keeling approach are still a good approximation of the artificial data sets ($r^2 \geq 94\%$, Figs. 5b, d). However, the y-axis intercept varies depending on the assumed δ^{13}C signal of the anthropogenic carbon flux and the mode of the terrestrial biosphere (active/passive) between −9.2‰ and −15.7‰, while the Law Dome data which contain these anthropogenic effects show −13.1‰ (Fig. 1b). Note, that these numbers are significantly higher than the isotopic signature of the anthropogenic carbon added to the system. Due to the non-negligible effect of a third reservoir, the ocean, the Keeling y-axis intercept deviates from the expected flux signature as discussed in Sect. 4. The difference to an ideal Keeling plot, in which the whole signal would be explained by the y-axis intercept has to be explained purely by oceanic uptake in the case of a passive terrestrial biosphere, and by a mixture of terrestrial and oceanic uptake in simulations with an active terrestrial biosphere.

Natural changes in atmospheric CO_2 over the past 650 000 years as recorded in Antarctic ice core records (Petit et al., 1999; Siegenthaler et al., 2005) were always slower and smaller in amplitude than the anthropogenic impact of the last 250 years. Therefore it is conservative to assume that the

oceanic uptake of a terrestrial disturbance in the past will always be greater than during the period influenced by human activity. We may therefore expect that the y-intercepts of a Keeling plot analysis of these glacial/interglacial processes are closer to the effective isotopic signature calculated from theory than the y_0 of data for the past few centuries.

5.3 Glacial/interglacial times

There are two factors that make a comparison of artificial time series with long ice core data sets difficult: First, the air which is enclosed in bubbles in the ice can circulate through the firn down to the depth where bubble close off occurs ($\sim 70-100$ m) before it is entrapped in the ice. The bubble close off is a slow process with individual bubbles closing at different times and depths. Accordingly the air enclosed in bubbles and in an ice sample is subject to a wide age distribution acting as an efficient low-pass filter on the atmospheric record. Therefore, all information from the gaseous components of the ice cores is averaged over a time interval of the age of the firn/ice transition zone. This time interval is depending on temperature and accumulation rates, but can roughly be estimated by the ratio of the depth of the firn/ice transition zone divided by the accumulation rate (Schwander and Stauffer, 1984). At Law Dome, the time integral is over a short period only (<20 years) (Etheridge et al., 1996); at Taylor Dome, it varies between 150 years during the Holocene and 300 years at the LGM (Steig et al., 1998a,b); at EPICA Dome C, where the most recent CO_2 and $\delta^{13}C$ measurements come from (Monnin et al., 2001; Eyer et al., 2004; Siegenthaler et al., 2005), it ranges between 300 and 600 years (Schwander et al., 2001). Second, the CO_2 and $\delta^{13}C$ records retrieved from ice cores are never continuous records, but consist of single measurements with large, but irregular gaps in between. In the Taylor Dome ice core these gaps are on average approximately 1000 years wide. It will therefore be of interest to investigate if the temporal resolution in the data set will be sufficient to resolve information potentially retrievable through the Keeling plot approach.

Anthropogenic activities add carbon via land use change and fossil fuel emissions to the atmosphere. The released carbon is only subsequently absorbed by the ocean. The causes for natural changes in atmospheric CO_2 during glacial/interglacial times were to a large extent located in the ocean. Thus, the causes and effects of anthropogenic and natural perturbations of the carbon cycle (including their timing) are in principle different. For the natural glacial/interglacial variations the carbon content of the atmosphere is determined by the surface ocean, the atmosphere is also called "slave to the ocean", while for the anthropogenic impact the opposite is the case.

This situation has also consequences for the investigation of different processes causing natural changes in the carbon cycle. We concentrate in the following on the individual impacts of seven important processes. These processes are changes in terrestrial carbon storage, export production of the marine biota, gas exchange rates and their variation through variable sea ice cover, ocean circulation, the physical effects of variable sea level and ocean temperature, and $CaCO_3$ sedimentation and dissolution. Please note, that in these factorial scenarios all processes can be treated un-coupled in our box model, e.g. changes in the circulation scheme will not lead to temperature variations, which might be the case in general circulation models. A summary of the long-term effects during Termination I of all these single process analyses is compiled in Table 2. Here, however, we discuss only the first three processes in greater detail. They are valuable examples of different variability in the carbon cycle: (1) Only the changing terrestrial carbon storage strictly resembles the initial idea of a Keeling plot (addition/subtraction of carbon from the atmosphere). (2) Changes in the marine biota illustrate how variations in the oceanic carbon cycle affects the atmospheric reservoirs. (3) The investigation of the gas exchange rates, finally, exemplifies a case in which the interface between atmosphere and ocean is perturbed.

5.3.1 Terrestrial biosphere

There are two opposing changes in terrestrial carbon storage to be investigated: carbon uptake and carbon release. Both might happen very fast in the course of abrupt climate anomalies, such as so-called Dansgaard/Oeschger events (Dansgaard et al., 1982; Johnsen et al., 1992), during which Greenland temperatures rose and dropped by more than 15 K in a few decades during the last glacial cycle (Lang et al., 1999; Landais et al., 2004). Terrestrial carbon storage anomalies during these events were estimated with a dynamic global vegetation model to be of the order of $50-100$ PgC (Köhler et al., 2005b). The time scales of these anomalies are of the order of centuries to millenia. We first analyse a scenario in which 10 PgC are released or taken up by the terrestrial pools within one year. This short time frame of one year was chosen to provide baseline experiments, in which the whole carbon flux is first altering the atmospheric reservoir, before oceanic uptake or release responds after year one. The amplitude of the perturbations is optimised to 10 PgC to guarantee still negligible numerical uncertainties (<0.01‰) in the calculation of the $\delta^{13}C$ fluxes. We follow with an experiment of linear carbon release to investigate the importance of the time scale for the Keeling plot interpretation. Results of scenarios of carbon uptake during Termination I as assumed in Köhler et al. (2005a) are very similar to the linear experiment and not discussed in greater detail.

Fast terrestrial carbon release

This is the scenario that comes closest to the original Keeling plot analysis in terrestrial ecosystem research. There is a source (terrestrial biosphere) which emits CO_2

Table 1. Terrestrial carbon release of different amplitude and isotopic signature and calculated y-axis intercept based on the original model output, after low-pass filtering of the data with a 300 year running mean, and after data filtering and reducing the data sets to samples every 100 years.

Scenario		y-axis intercept of different regression models (‰) (r^2 (%) in brackets)	
Amplitude of the release (PgC)	isotopic signature $\delta^{13}C_{rel}$ of release (‰)	model 1 rising[a]	model 2 prior – after[b]
original model output			
10	−23.4	−23.8 (100)	−8.4 (100)
5	−23.4	−23.6 (100)	−8.4 (100)
10	−33.4	−33.9 (100)	−9.3 (100)
10	−13.5	−13.6 (100)	−7.5 (100)
300 yr running mean			
10	−23.4	−8.9 (93)	−8.4 (100)
5	−23.4	−8.9 (93)	−8.4 (100)
10	−33.4	−10.2 (92)	−9.3 (100)
10	−13.5	−7.7 (95)	−7.5 (100)
300 yr running mean + data selection every 100 yr			
10	−23.4	−8.6 (100)	−8.4 (100)
5	−23.4	−8.6 (100)	−8.4 (100)
10	−33.4	−9.6 (100)	−9.3 (100)
10	−13.5	−7.5 (97)	−7.5 (100)

[a] This covers data during rise of atmospheric pCO_2, which are only two points in the original data set, but longer series in smoothed records.
[b] Comparing steady state before with new steady state after carbon release.

Table 2. Summary of y-axis intercept y_0 of the prior/after Keeling plot analysis (regression model 2) for processes changing over Termination I. The third column classifies the processes according to their y_0 into groups.

Process	y_0 (‰)	Group
Linear rise in terrestrial carbon storage	−8.6	I
Decrease in marine export production	−8.6	I
Rise in Southern Ocean vertical mixing	−8.2	II
Rise in NADW formation	−7.8	II
Rise in sea level	−6.4	III
Rise in temperature	−3.6	III
Decline in sea ice cover/rise in gas exchange rates	−0.7	IV

directly into the atmosphere. In this experiment, atmospheric pCO_2 is first increased by more than 4 μatm immediately after the release of 10 PgC, and then stabilises again at a value less than 1 μatm above the initial one (Fig. 6a). The $\delta^{13}C$ signal shows a drop by more than 0.3‰ in year one, and a steady state which is nearly similar to the initial situation (Fig. 6a). Near steady state (±0.1%) in both pCO_2 and $\delta^{13}C$ was reached 376 years after the carbon release.

There are two straightforward possibilities to draw a regression function through the Keeling plot (Fig. 6b):

1. A line connecting only the data just before the start of the carbon release experiment (year 0) and one year later after 10 PgC got released but before any carbon has been taken up by the ocean; this line will present the maximum possible slope. Thus, pCO_2 and $\delta^{13}C$ after the release can also be calculated following the mass balance equations of the two reservoir system (Eqs. 3 and 4).

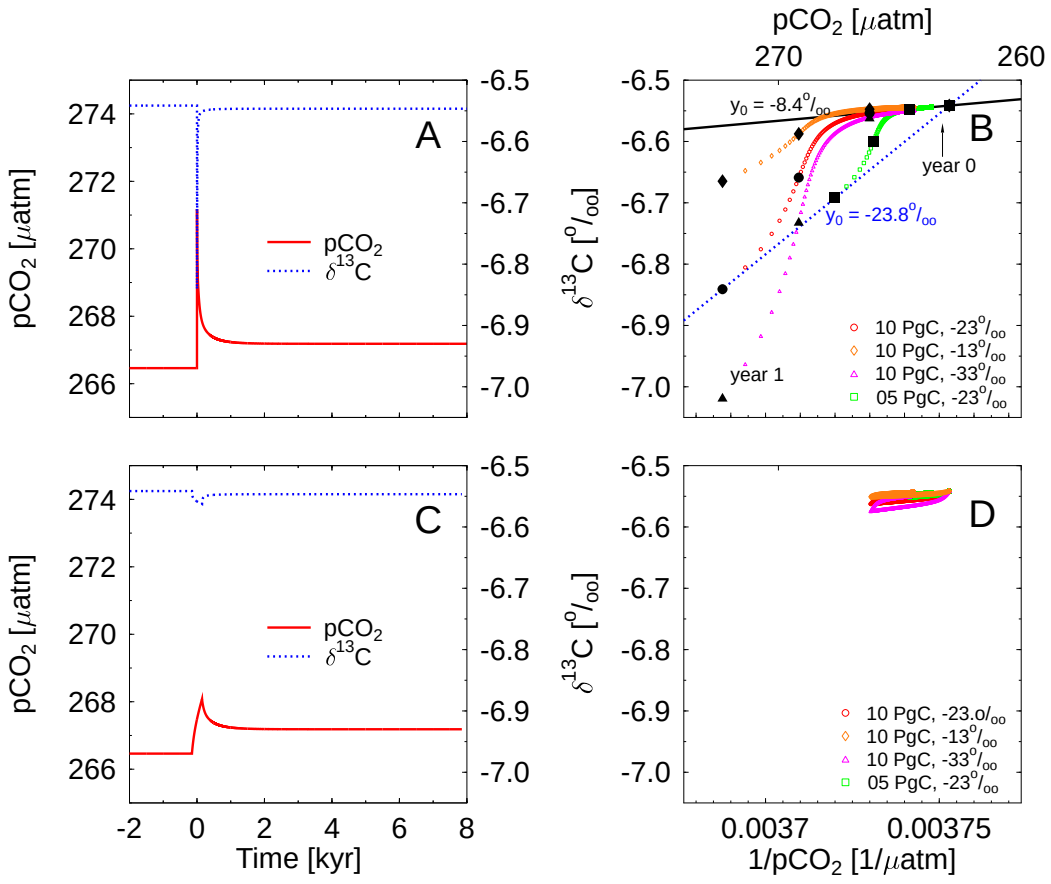

Fig. 6. Effect of a pulse of instantaneous release (within one year) of terrestrial carbon with an isotopic signature of $\delta^{13}C = -23‰$ (left: pCO_2, $\delta^{13}C$; right: Keeling plot). Different carbon release amplitudes (5, 10 PgC) and different $\delta^{13}C$ signatures ($-13‰$, $-23‰$, $-33‰$) are tested. The regression functions seen in **(b)** are for the two different regression models for the 10 PgC/$-23‰$ scenario (red circles). Model 1: year 0 and year 1 (short dash); model 2: year 0 and year 8000 (solid); Large black markers mark the years 0, 1, 10, 100 in each record. Bottom: Same as above but now the data are smoothed with a 300 yr running mean.

2. A straight line through two points characterising the states prior to the carbon release and after re-equilibration. This would contain the minimum information retrievable in case of low sampling frequency and would be an analogy to the theoretical considerations for a three reservoir system.

If such an event of terrestrial carbon release is to be detected in ice cores, we have to process our artificial data set to account for both the temporal integral during gas enclosures and the limited sampling frequency. We assumed an average mixing time (running average of 300 years), and a regular sampling frequency of 100 years, typical for Antarctic ice core studies.

A summary of the calculated y-axis intercepts is given in Table 1. In the original model output, the regression model 1 (analysis of the carbon flux in the year of the release) can explain the $\delta^{13}C$ signature of terrestrial release very well. The slight overestimation of the regression model of up to $0.5‰$ might be due to numerical limitations. In model 2 the different y-axis intercept ($y_0 = -8.6‰$) is similar to the limiting value $\delta^{\Delta A}_{\delta B \to 0}$ introduced in Sect. 4, which is an embedded feature of the system configuration. This can be understood from the analysis of Fig. 3a and Table 1 in the following way: The functional dependency of $\delta^{\Delta A}_{\delta B \to 0}$ from the amplitude of the carbon release is small. A release of 10 and 5 PgC yields to similar y_0's in the prior/after regression model. It is expected that y_0 is unchanged for even smaller perturbations ($B \to 0$). It is therefore a recorder of the system configuration, similar as $\delta^{\Delta A}_{\delta B \to 0}$ for the numerical development of the three reservoir approach. Interestingly, the y_0 values derived from the BICYCLE simulations are about $1‰$ isotopically heavier than in our theoretical model in Sect. 4. The reason for this is the establishing of vertical gradients in DIC and $\delta^{13}C$ in the ocean due to the ocean carbon pumps (Volk and Hoffert, 1985) leading to an enrichment of $\delta^{13}C$ in the surface water by about $1‰$.

If we take the signal broadening through temporal mixing in the firn into account (Fig. 6 bottom), the perturbations

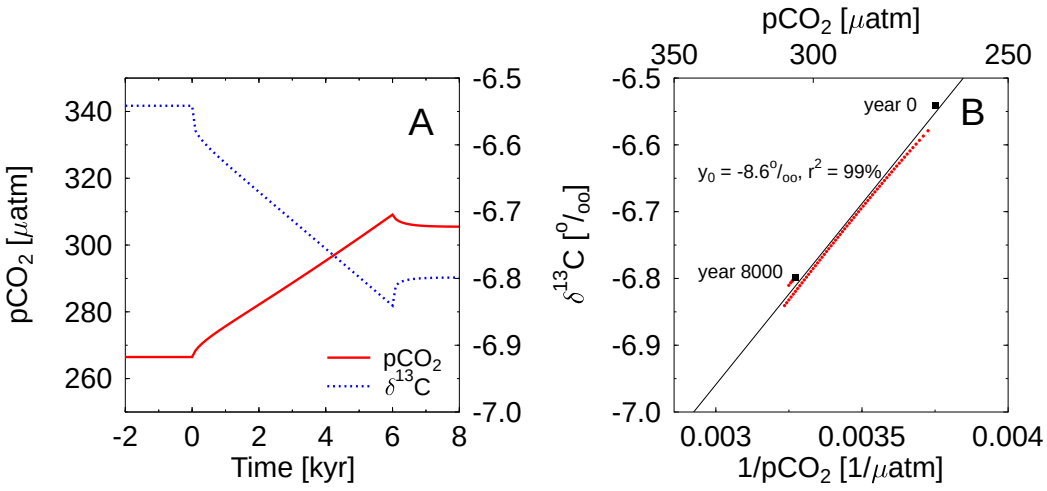

Fig. 7. Effects of a linear decrease in terrestrial carbon storage by 500 PgC (left: pCO_2, $\delta^{13}C$; right: Keeling plot). Regressions in the Keeling plots are performed over the whole time period.

in pCO_2 and $\delta^{13}C$ are largely reduced to 34% and 7% of their original amplitudes, respectively, and the duration of the atmospheric pCO_2 rise of one year in the original data is now spread over the time length of the smoothing filter (300 yr). Even for conditions similar to those found at Law Dome where the air is mixed only over a time interval of 20 years, the amplitudes in pCO_2 and $\delta^{13}C$ are reduced to 70% and 47% of their original values, respectively. The y-axis intercepts for the 300 year smoothing filter are reduced significantly for regression model 1 (30% to 57% of y_0 in original data).

A further change arises if we reduce the sampling interval. The effect of a 100 year sampling frequency reduces y-axis intercepts calculated with regression model 1 further (Table 1). However, the change introduced by reduced sampling frequency is much smaller than the one based on firn air mixing. Results obtained with regression model 2 (limiting value $\delta^{\Delta A}_{\delta B\rightarrow 0}$) were not affected by any of the two post simulation procedures.

From these fast carbon release experiments, several conclusions can be drawn:

1. The results of regression model 1 are in line with the mass balance equations of the two reservoir Keeling approach.
2. In all multi-annual experiments the oceanic uptake of carbon will play an important role.
3. Fast terrestrial carbon release events are in their full extent not recordable in the ice core records due to the time integral introduced by the firn enclosure process, i.e. only the net change after equilibration of the ocean/atmosphere system can be deduced as in regression model 2. In the following we will therefore concentrate our discussion on this prior/after analysis.

Slow terrestrial carbon exchange

To understand glacial/interglacial dynamics one has to investigate larger variations in terrestrial carbon storage of several hundreds of PgC, which occurred over longer time intervals. We have therefore performed an additional experiment, in which 500 PgC is released by the terrestrial pools, but now with a constant release rate over a period of 6000 years.

In the experiment the atmospheric $\delta^{13}C$ record shows a relaxation behaviour in the first several hundred years after the beginning and after the end of the carbon release with a gradual change in between (Fig. 7). Atmospheric pCO_2 is changing rather constantly over time, also with small non-linear responses in the first few hundred years at the beginning and at the end of the experiment. These discontinuities are caused by the time-delayed oceanic carbon uptake. For example, after the end of the experiment (t=6 kyr, Fig. 7a) a large part is taken up by the ocean in the following centuries, similar as in the fast carbon release experiment shown in Fig. 6. In the Keeling plot the relaxation behaviour at the beginning and the end of the linear experiments leads to offsets from the well defined linear relationship. A regression over the whole time period as well as the prior/after analysis (regression model 2) leads to y_0=−8.6‰.

The $\delta^{13}C$ value in our simulation result for a slow terrestrial carbon release agrees well with the one proposed by our theoretical three reservoir approach in Sect. 4 and is very different from the original $\delta^{13}C$ of the carbon source. It is especially remarkable that the differences between y_0 and $\delta^{\Delta A}_{\delta B\rightarrow 0}$ are very small. Furthermore, these carbon exchange processes are so slow that the air enclosure procedure with the assumed smoothing filter of 300 years would only marginally alter the records and would not change the y_0 values. Sim-

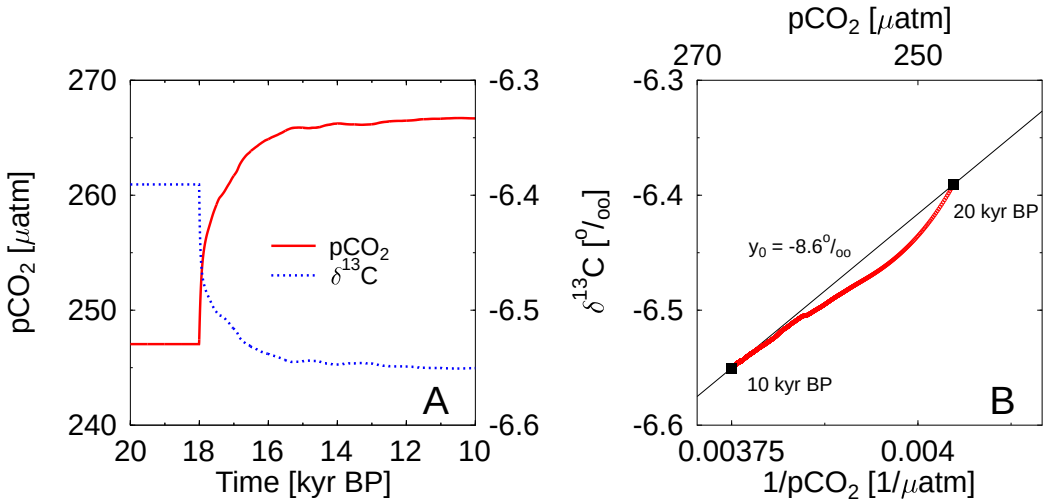

Fig. 8. Effects of iron fertilisation in the Southern Ocean on atmospheric carbon records with scenario taken from Köhler et al. (2005a) ((**a**): pCO_2, $\delta^{13}C$; (**b**): Keeling plot).

ilarly, the restricted sampling frequency is of no importance here. These two processes will therefore not be analysed any further in the following, because it is reasonable to assume that their impact on the observed processes can be neglected.

5.3.2 Marine biosphere

While the marine biosphere is in principle a reservoir separate from DIC in the ocean, it is not independent because the marine export production exerts a strong control on the vertical gradients in DIC and $\delta^{13}C$ between the surface and the deep ocean. Accordingly, the following discussion of changes caused by the marine biosphere and other factors represents already a misuse of the Keeling plot approach. It is nevertheless instructive to study whether this analysis can lead to meaningful results and is able to distinguish between different processes.

For the marine biota we analyse one scenario which seems to be realistic for the last glacial/interglacial transition. In this scenario the possible effect of an enhanced glacial marine productivity due to the iron fertilisation in the Southern Ocean is explored. In the preindustrial ocean a flux of 10 PgC yr^{-1} of organic carbon is exported at 100 m water depth to the deeper ocean. This organic export production is coupled via the rain ratio to an export of 1 PgC yr^{-1} of inorganic $CaCO_3$. The marine export flux during the LGM is about 12 PgC yr^{-1}. The increase is assumed to be caused by increase aeolian iron input in the Southern Ocean which then mobilises un-utilised nutrients for additional export production. During the transition (18 to 10 kyr BP) the enhanced marine export flux is reduced to its preindustrial value through coupling to the reduced iron flux measured in Antarctic ice cores.

The iron fertilisation experiment decreases glacial pCO_2 by 20 μatm, in parallel with a 0.15‰ rise in $\delta^{13}C$ (Fig. 8a). Both atmospheric carbon records are relaxing to their preindustrial values after the onset of iron limitation around 18 kyr BP. With the prior/after model the Keeling plot leads to a y_0=−8.6‰ (Figs. 8b). Note, that this value is identical to the one derived for the terrestrial carbon release experiment and reflects the similar fractionation during marine photosynthesis.

The marine export production combines two of the three ocean carbon pumps: the organic or soft-tissue pump and the carbonate pump (Volk and Hoffert, 1985). The third one, the solubility pump, operates by the increased solubility of CO_2 in downwelling cold water. They all introduce vertical gradients in DIC in the water column, the biological pumps additionally build up a gradient in $\delta^{13}C$. DIC is reduced in the surface layers through marine production of both organic material (soft-tissues) and $CaCO_3$ and increased in the abyss through carbon released during remineralisation and dissolution. During photosynthesis $\delta^{13}C$ is depleted by about −20‰, thus leaving carbon enriched in ^{13}C at the surface, while the exported organic matter is depleted. The isotopic fractionation during the production of hard shells slightly enriches ^{13}C in the carbonate (ε=0‰ to 3‰). In BICYCLE the flux of CO_2 from the surface ocean to the atmosphere has a fractionation factor of $\varepsilon_{O2A}\approx-10.4$‰ and $\varepsilon_{A2O}\approx-2.4$‰ in the opposite direction leading to a net fractionation effect of −8.0‰ (but both depend also on temperature, and ε_{O2A} additionally on DIC, HCO_3^-, and CO_3^{2-}). The signal seen in the atmospheric record is therefore a composite of the fractionation during gas exchange and an increased carbon flux from the atmosphere to the ocean. Systematic deviations from the prior/after regression line are due to slow equilibration processes in the ocean/atmosphere system.

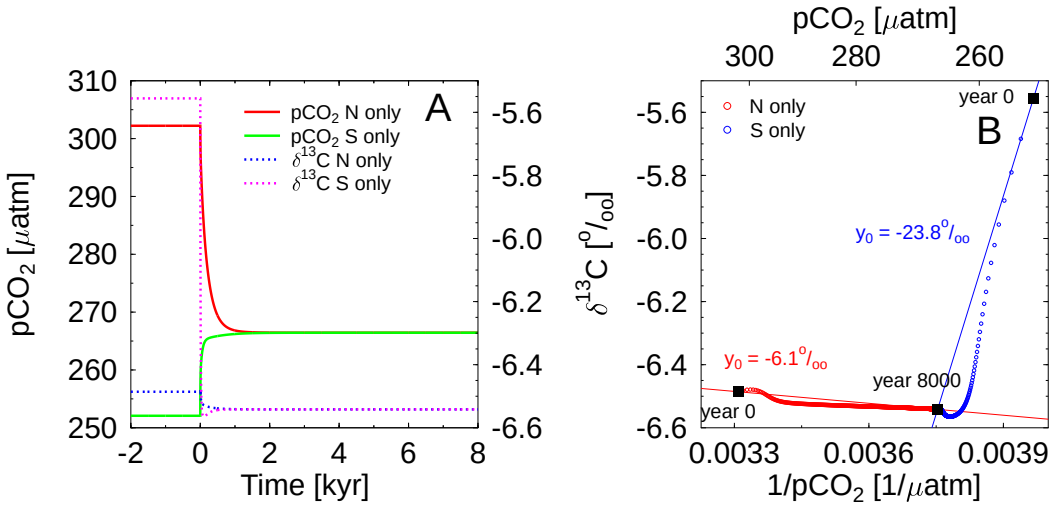

Fig. 9. Simulated effects of an instantaneous change in sea ice cover from total coverage to preindustrial values in the North Atlantic (N only), or the Southern Ocean (S only) (left: pCO_2, δ^{13}C; right: Keeling plot).

5.3.3 Gas exchange/sea ice

A change in sea ice cover leads to changes in the gas exchange rates with opposing effects for the northern and the southern high latitudes. As the preindustrial North Atlantic Ocean is a sink for CO_2 a reduced gas-exchange due to more extended sea ice cover leads to rising atmospheric pCO_2, while the same happening in the Southern Ocean being a source for CO_2 leads to a drop in pCO_2. We explore the maximum amplitudes possible by covering either the whole North Atlantic Ocean or Southern Ocean surface boxes with sea ice, reducing the gas exchange rates in these areas to zero (Fig. 9).

In these extreme scenarios sea ice cover is relaxed instantaneously from a full coverage of the surface ocean boxes to preindustrial areal distribution in year 0. The experiment in the North Atlantic yields a drop in pCO_2 by 35 μatm, a drop in δ^{13}C by 0.04‰, and a y-axis intercept (prior/after analysis) in the Keeling plot analysis of -6.1‰. A similar experiment in the Southern Ocean increases pCO_2 by about 15 μatm, δ^{13}C drops by 1.0‰ leading to a prior/after y-axis intercept of -23.8‰.

The very negative y_0 caused by changes in sea ice coverage in the Southern Ocean needs further clarification. The changes in sea ice coverage cause variations in the gas exchange rates. In a scenario resampling plausible changes in sea ice across Termination I (Köhler et al., 2005a, 2006b), the global exchange flux rises from 52 PgC yr^{-1} during the LGM to 58 PgC yr^{-1} at t=10 kyr BP in the scenario, which considers only changes in sea ice in the Southern Ocean. The pCO_2 of the atmosphere and the Southern Ocean surface box are very close to each other at the beginning of the experiment (270 and 266 μatm, respectively). Therefore, an increase in gas exchange rate in the Southern Ocean is only marginally increasing atmospheric pCO_2($<$1 μatm). However, the stronger gas exchange leads to a significant decrease in atmospheric δ^{13}C by 0.08‰. A y_0 of -77.2‰ caused by a plausible reduction in Southern Ocean sea ice cover over Termination I is consistent in our modelling environment, but dependent strongly on the model architecture. In general, the effects of sea ice coverage on carbon cycle dynamics have been found to vary between different models (Archer et al., 2003). This example shows, that the Keeling plot is difficult to interpret for experiments without significant net carbon exchange with the atmosphere, but where there are still changes in atmospheric δ^{13}C. The slope of the regression function might in the most extreme case of a constant pCO_2 rise to infinity. Besides gas exchange a second example for this situation is a change from C3 grasses to C4 grasses in the terrestrial biosphere. With these realistic changes in sea ice cover across Termination I the prior/after analysis yields a y_0 of -0.7‰ (Table 2).

5.3.4 Other processes

Other processes which change the oceanic carbon cycle (ocean circulation, sea level, ocean temperature) are not discussed in detail. We briefly summarise the assumptions underlying these processes and their consequences for a Keeling plot analysis in the following, but refer the readers for more information to Köhler et al. (2005a, 2006b). The y-intercepts of the prior/after analysis of these processes are all within the range spanned by the results of the previously discussed changes (Table 2). The sediment/ocean interaction (carbonate compensation) is a special case. The influence of the fluxes of $CaCO_3$ cannot be analysed separately as $CaCO_3$ fluxes between deep ocean and sediment are generated by the model as response to changes in the deep ocean CO_3^{2-} concentration. Carbonate compensation is acting as an amplifier of the results of all other processes with re-

spect to the changes in pCO_2. It is therefore not possible to find a pure signal of carbonate compensation in atmospheric records. The impact of this process could in principle be estimated by subtracting results of simulations, in which carbonate compensation is either on or off from each other, but we refrain from this. All other process analyses (including terrestrial and marine biota and sea ice) were performed without carbonate compensation.

In general, it has to be said that especially abrupt changes in ocean circulation lead to fast fluctuations in both atmospheric carbon records and thus also to Keeling plots, which are not easily represented by linear regression models. However, our comparison here is restricted to the long-term effects, in which atmosphere and ocean are already equilibrated.

Ocean circulation:
Based on evidences from various sediment records and ocean general circulation models we assume changes (1) in the strength of the North Atlantic Deep Water (NADW) formation and (2) in the Southern Ocean vertical mixing. (1): NADW formation is increased from its glacial strength (10 Sv) during the LGM to intermediate levels of 16 Sv at the beginning of the Holocene neglecting potential millennial scale fluctuations during the Bølling/Allerød and Younger Dryas climate anomalies. This leads to a rise in atmospheric pCO_2 by 12 μatm and a small drop in $\delta^{13}C$ (-0.06‰). The prior/after analysis in the Keeling plot leads to a y-axis intercept of -7.8‰. (2): Southern Ocean vertical mixing rate rises from 9 Sv (LGM) to 29 Sv (Holocene) and leads to a rise in pCO_2 by about 30 μatm and a drop in $\delta^{13}C$ by more than 0.2‰. Here, the Keeling plot interpretation gives us a y-axis intercept of -8.2‰ for the prior/after analysis.

The overturning circulation distributes carbon in the ocean. Its effect on the atmospheric carbon reservoirs, however, is opposite to that of the three ocean carbon pumps. While the pumps introduce vertical gradients in DIC and $\delta^{13}C$, the overturning circulation is reducing these vertical gradients again through the ventilation of the deep ocean which brings water rich in DIC and depleted in ^{13}C back to the surface. A weakening of the ventilation reduces these upwelling processes and leads to lower pCO_2 and higher $\delta^{13}C$ values as seen in the experiments.

Sea level:
Sea level rose from 20 kyr BP to 10 kyr BP by about 85 m. This leads in our model to a drop in pCO_2 by about 13 μatm and nearly no change in the $\delta^{13}C$. The y-axis intercept in a Keeling plot with prior/after analysis or regression over whole time period is -6.4‰.

The rising sea level leads to a dilution of the concentration of all species in the ocean and a decrease in salinity by about 2.3%. The ocean can then store more carbon.

Ocean temperature:
The rise of the ocean temperature by 3 to 5 K during the simulated 20 to 10 kyr BP leads to a rise in pCO_2 of 32 μatm, and a rise in $\delta^{13}C$ of 0.4‰, the latter leading the first by about 1000 years. The Keeling plot analysis gives us a y_0 of -3.6‰ for the regression in the prior/after analysis.

Due to the temperature dependent solubility of CO_2 warm water stores less carbon than cold water. A rise in ocean temperature therefore weakens the solubility pump and leads to an out-gassing of CO_2. The rise in $\delta^{13}C$ is mainly caused by the temperature-dependent isotopic fractionation during gas exchange between the surface ocean and the atmosphere.

6 Conclusions

In this study we analysed processes which alter the atmospheric content of carbon dioxide and $\delta^{13}C$ of CO_2 using artificial time series produced with a global carbon cycle box model. For the investigation of these artificial time series and their potential to be interpreted using the Keeling plot approach, the absolute validity of our simulation scenarios is not important. By using a simple carbon cycle model we benefit from the fact that individual processes acting on the carbon cycle can be switched on and off and their hypothetical impacts can be analysed individually. We furthermore developed a theoretical framework to extend the application of the Keeling plot approach to long-term effects of terrestrial carbon release.

All processes have been analysed with respect to their impact to the Keeling plot analysis. A summary is found in Table 2. The y-intercepts of this analysis in the case of terrestrial carbon release is fundamentally different from the expected value, which should contain the $\delta^{13}C$ of the terrestrial source. The bias can be understood based on theoretical considerations of a three reservoir system which also includes oceanic carbon uptake. These considerations are the paleo extension of the Keeling plot approach to envisage long-term effects of terrestrial processes. From them $\delta^{\Delta A}$ is calculated, the long-term change in the isotopic signature of atmospheric CO_2 caused by the underlying process, called *effective isotopic signature*. $\delta^{\Delta A}_{\delta B \to 0}$ obtained from theory is comparable to the y-axis intercept y_0 in a classical Keeling plot. So far, changes in the marine carbon cycle can not be understood with our simple three reservoir approach.

However, the comparison of y-intercepts derived from different processes is used to investigate if this method can be used to distinguish between different processes operation on long time scales on the global carbon cycle. The y_0's of the prior/after analysis of our single process analysis vary between -0.7 and -8.6‰. Based on the calculated y_0 values the processes can be subdivided into four groups (Table 2): (I) Processes in which the biology is involved (marine and terrestrial) have identical y_0's (-8.6‰) and are therefore in-

distinguishable. (II) Changes in the ocean circulation lead to y_0's which are slightly more positive (-7.8 to -8.2‰). Processes belonging to the groups I and II might in real data sets also be indistinguishable due to measuremental uncertainties. (III) Sea level (-6.4‰) and ocean temperature (-3.6‰) have in their long-term behaviour intermediate y_0's, clearly higher than those of the first two groups. (IV) Gas exchange/sea ice cover yields to the highest y_0, but it should be kept in mind that this process is a compound of subprocesses which have distinctively different y_0 values (sea ice cover in different hemispheres, y_0 (north)=-4.8‰; y_0 (south)=-77.2‰). Furthermore, the terrestrial carbon storage very likely changed in a non-linear way during the last glacial/interglacial transition and not in a linear way as assumed here. This is also supported by a simulation studies using a dynamical global vegetation model (Köhler et al., 2005b). High frequency changes on a centennial to millennial time scale are very likely smoothed out in the ice core records due to the average mixing time of the air of several centuries and the limited sampling frequency.

From the understanding which emerges here, it seems unlikely, that the interpretation of δ^{13}C measured during glacial/interglacial transitions can be enhanced very much with the Keeling plot approach. The identification of a single process which might be responsible for the observed fluctuations in atmospheric CO_2 and δ^{13}C can not be based on a Keeling plot analysis. Most processes acted simultaneously on the global carbon cycle during the transition and the uncertainties in data retrieval, y-axis intercept, and δ^{13}C are too large to come to a sound and unequivocal process identification.

Appendix A Calculating the effective isotopic signature of the three reservoir system

The effective isotopic signature $\delta^{\Delta A}$ of the perturbation B, defined by Eq. (10) from Sect. 4

$$\delta^{\Delta A} = \frac{A\delta^A - A_0\delta_0^A}{A - A_0}$$

can be rewritten such that it is only a function of the initial values (A_0, O_0, δ_0^A, δ_0^O), the forcing (B, δ^B) and parameters (β, $\varepsilon_{\mathrm{AO}}$). To start, Eq. (10) is rewritten under the equivalent expression

$$\delta^{\Delta A} = \delta_0^A + \frac{A}{A - A_0}(\delta^A - \delta_0^A) \tag{A1}$$

The reformulation then proceeds in two stages, the first one dealing with $A/(A - A_0)$, the second one with $(\delta^A - \delta_0^A)$.

For the first stage, we start by rewriting and combining Eqs. (6) and (9) into a linear system of equations in the anomalies $(A - A_0)$ and $(O - O_0)$

$$(O - O_0) + (A - A_0) = B$$
$$\beta\frac{A_0}{O_0}(O - O_0) - (A - A_0) = 0$$

The solutions of this system are

$$O - O_0 = B\frac{1}{\beta\frac{A_0}{O_0} + 1} \tag{A2}$$

and

$$A - A_0 = B\frac{\beta\frac{A_0}{O_0}}{\beta\frac{A_0}{O_0} + 1}. \tag{A3}$$

To conclude the first stage, it is sufficient to rewrite $A/(A - A_0)$ as

$$\frac{A}{A - A_0} = \frac{A_0}{A - A_0} + 1, \tag{A4}$$

and use (A3) to replace $(A - A_0)$. After reduction and simplification, we find that

$$\frac{A}{A - A_0} = \frac{A_0 + \frac{O_0}{\beta} + B}{B}. \tag{A5}$$

The second stage proceeds from Eq. (7)

$$A\delta^A + O\delta^O = A_0\delta_0^A + O_0\delta_0^O + B\delta^B,$$

where we first substitute $\delta^O = \delta^A - \epsilon_{AO}$ and $\delta_0^O = \delta_0^A - \epsilon_{AO}$. After collecting the terms in δ^A, δ_0^A and ϵ_{AO} we then get

$$(A + O)\delta^A - (A_0 + O_0)\delta_0^A - (O - O_0)\epsilon_{AO} = B\delta^B.$$

To continue, we substitute $\delta^A = (\delta^A - \delta_0^A) + \delta_0^A$ and rearrange to get

$$(A + O)(\delta^A - \delta_0^A) - (O - O_0)\epsilon_{AO} + ((A + O) - (A_0 + O_0))\delta_0^A = B\delta^B.$$

We then use Eqs. (6)

$$A + O = A_0 + O_0 + B$$

and (A2) to substitute $(A + O)$ and $(O - O_0)$ respectively. After simplification, we get

$$(A_0 + O_0 + B)(\delta^A - \delta_0^A) = B(\delta^B - \delta_0^A + \frac{\epsilon_{AO}}{\beta\frac{A_0}{O_0} + 1}),$$

from which we may immediately deduce that

$$\delta^A - \delta_0^A = \frac{B}{A_0 + O_0 + B}\left(\delta^B - \delta_0^A + \frac{\epsilon_{AO}}{\beta\frac{A_0}{O_0} + 1}\right). \tag{A6}$$

Finally, by insertion of Eqs. (A5) and (A6) into (A1) we obtain the desired expression

$$\delta^{\Delta A} = \delta_0^A + \left(\delta^B - \delta_0^A + \frac{\varepsilon_{\mathrm{AO}}}{\beta\frac{A_0}{O_0} + 1}\right)\frac{A_0 + \frac{O_0}{\beta} + B}{A_0 + O_0 + B}. \tag{A7}$$

Acknowledgements. We thank J. Severinghaus for ideas on the three box model calculations, J. Freitag for discussions on firnification and bubble close off, J. Bijma for his editorial effort and two anonymous referees for their clarifying comments. This study is funded by the German Ministry of Education and Research through the German Climate Research Programme DEKLIM (project RESPIC). G. Munhoven is a Research Associate with the Belgian National Fund for Scientific Research (FNRS).

Edited by: J. Bijma

References

Archer, D. E., Martin, P. A., Milovich, J., Brovkin, V., Plattner, G.-K., and Ashendel, C.: Model sensitivity in the effect of Antarctic sea ice and stratification on atmospheric pCO_2, Paleoceanography, 18, 1012, doi:10.1029/2002PA000760, 2003.

Blasing, T. J., Broniak, C., and Marland, G.: Estimates of monthly carbon dioxide emissions and associated $\delta^{13}C$ values from fossil-fuel consumption in the U.S.A, in: Trends: A Compendium of Data on Global Change, Carbon Dioxide Information Analysis Center, Oak Ridge National Laboratory, U.S. Department of Energy, Oak Ridge, Tenn., USA, 2004.

Bowling, D. R., Tans, P. P., and Monson, R. K.: Partitioning net ecosystem carbon exchange with isotopic fluxes of CO_2, Global Change Biol., 7, 127–145, 2001.

Brook, E. J., Harder, S., Serveringhaus, J., Steig, E. J., and Sucher, C. M.: On the origin and timing of rapid changes in atmospheric methane during the last glacial period, Global Biogeochem. Cycles, 14, 559–572, 2000.

Dansgaard, W., Clausen, H. B., Gundestrup, N., Hammer, C. U., Johnsen, S. F., Kristinsdottir, P. M., and Reeh, N.: A new Greenland deep ice core, Science, 218, 1273–1277, 1982.

Emanuel, W. R., Killough, G. G., Post, W. M., and Shugart, H. H.: Modeling terrestrial ecosystems in the global carbon cycle with shifts in carbon storage capacity by land-use change, Ecology, 65, 970–983, 1984.

Etheridge, D. M., Steele, L. P., Langenfelds, R. L., Francey, R. J., Barnola, J.-M., and Morgan, V. I.: Natural and anthropogenic changes in atmospheric CO_2 over the last 1000 years from air in Antarctic ice and firn, J. Geophys. Res., D101, 4115–4128, 1996.

Eyer, M., Leuenberger, M., Nyfeler, P., and Stocker, T.: Comparison of two $\delta^{13}CO_2$ records measured on air from the EPICA Dome C and Kohnen Station ice cores, Geophys. Res. Abstr., 6, 01 990, 2004.

Fischer, H., Wahlen, M., and Smith, J.: Reconstruction of glacial/interglacial changes in the global carbon cycle from CO_2 and $\delta^{13}CO_2$ in Antarctic ice cores, Memoirs of the National Institute for Polar Research, Special Issue, 57, 121–138, 2003.

Flanagan, L. B. and Ehleringer, J. R.: Ecosystem-atmosphere CO_2 exchange: interpretating signals of change using stable isotope ratios, Trends in Ecology and Evolution, 13, 10–14, 1998.

Francey, R. J., Allison, C. E., Etheridge, D. M., Trudinger, C. M., Enting, I. G., Leuenberger, M., Langenfelds, R. L., Michel, E., and Steele, L. P.: A 1000-year high precision record of $\delta^{13}C$ in atmospheric CO_2, Tellus, 51B, 170–193, 1999.

Friedli, H., Lötscher, H., Oeschger, H., Siegenthaler, U., and Stauffer, B.: Ice core record of the $^{13}C/^{12}C$ ratio of atmospheric CO_2 in the past two centuries, Nature, 324, 237–238, 1986.

Hemming, D., Yakir, D., Ambus, P., Aurela, M., Besson, C., Black, K., Buchmann, N., Burlett, R., Cescatti, A., Clement, R., Gross, P., Granier, A., Grünwald, T., Havrankova, K., Janous, D., Janssens, I. A., Knohl, A., Köstner, B., Kowalski, A., Laurila, T., Mata, C., Marcolla, B., Matteucci, G., Moncrieff, J., Moors, E. J., Osborne, B., Pereira, J. S., Pihlatie, M., Pilegaard, K., Ponti, F., Rosova, U., Rossi, F., Scartazza, A., and Vesala, T.: Pan-European $\delta^{13}C$ values of air and organic matter from forest ecosystems, Global Change Biol., 11, 1065–1093, doi:10.1111/j.1365–2486.2005.00 971.x, 2005.

Houghton, R. A.: Revised estimates of the annual net flux of carbon to the atmosphere from changes in land use and land management 1850–2000, Tellus, 55B, 378–390, 2003.

Johnsen, S. J., Clausen, H. B., Dansgaard, W., Fuhrer, K., Gundestrup, N., Hammer, C. U., Iversen, P., Jouzel, J., Stauffer, B., and Steffensen, J. P.: Irregular glacial interstadials recorded in a new Greenland ice core, Nature, 359, 311–313, 1992.

Keeling, C. D.: The concentration and isotopic abundance of carbon dioxide in rural areas, Geochim. Cosmochim. Acta, 13, 322–334, 1958.

Keeling, C. D.: The concentration and isotopic abundance of carbon dioxide in rural and marine air, Geochim. Cosmochim. Acta, 24, 277–298, 1961.

Keeling, C. D. and Whorf, T. P.: Atmospheric CO_2 records from sites in the SIO air sampling network, in Trends: A Compendium of Data on Global Change, Carbon Dioxide Information Analysis Center, Oak Ridge National Laboratory, U.S. Department of Energy, Oak Ridge, Tenn., USA, 2005.

Keeling, C. D., Bollenbacher, A. F., and Whorf, T. P.: Monthly atmospheric $^{13}C/^{12}C$ isotopic ratios for 10 SIO stations, in: Trends: A Compendium of Data on Global Change, Carbon Dioxide Information Analysis Center, Oak Ridge National Laboratory, U.S. Department of Energy, Oak Ridge, Tenn., USA, 2005.

Köhler, P. and Fischer, H.: Simulating changes in the terrestrial biosphere during the last glacial/interglacial transition, Global and Planetary Change, 43, 33–55, doi:10.1016/j.gloplacha.2004.02.005, 2004.

Köhler, P. and Fischer, H.: Simulating low frequency changes in atmospheric CO_2 during the last 740 000 years, Clim. Past, 2, 57–78, 2006, http://www.clim-past.net/2/57/2006/.

Köhler, P., Fischer, H., Munhoven, G., and Zeebe, R. E.: Quantitative interpretation of atmospheric carbon records over the last glacial termination, Global Biogeochem. Cycles, 19, GB4020, doi:10.1029/2004GB002345, 2005a.

Köhler, P., Joos, F., Gerber, S., and Knutti, R.: Simulated changes in vegetation distribution, land carbon storage, and atmospheric CO_2 in response to a collapse of the North Atlantic thermohaline circulation, Clim. Dyn., 25, 689–708, doi:10.1007/s00 382–005–0058–8, 2005b.

Köhler, P., Muscheler, R., and Fischer, H.: A model-based interpretation of low frequency changes in the carbon cycle during the last 120 000 years and its implications for the reconstruction of atmospheric $\Delta^{14}C$, Geochem., Geophys., Geosyst., 7, Q11N06, doi:10.1029/2005GC001228, 2006a.

Köhler, P., Schmitt, J., and Fischer, H.: On the application and interpretation of Keeling plots in paleo climatic research — Deciphering $\delta^{13}C$ of atmospheric CO_2 measured in ice cores, Bio-

geosciences Discuss., 3, 513–573, 2006b.

Landais, A., Barnola, J. M., Masson-Delmotte, V., Jouzel, J., Chappellaz, J., Caillon, N., Huber, C., Leuenberger, M., and Johnsen, S. J.: A continuous record of temperature evolution over a sequence of Dansgaard-Oeschger events during Marine Isotope Stage 4 (76 to 62 kyr BP), Geophys. Res. Lett., 31, L22 211, doi:10.1029/2004GL021193, 2004.

Lang, C., Leuenberger, M., Schwander, J., and Johnsen, S.: 16°C rapid temperature variation in central Greenland 70,000 years ago, Science, 286, 934–937, 1999.

Levin, I., Ciais, P., Langenfelds, R., Schmidt, M., Ramonet, M., Sidorov, K., Tchebakova, N., Gloor, M., Heimann, M., Schulze, E.-D., Vygodskaya, N. N., Shibistova, O., and Lloyd, J.: Three years of trace gas observations over the EuroSiberian domain derived from aircraft sampling – a concerted action, Tellus, 54B, 696–712, 2002.

Marland, G., Boden, T., and Andres, R. J.: Global, Regional, and National CO_2 Emissions, in Trends: A Compendium of Data on Global Change, Carbon Dioxide Information Analysis Center, Oak Ridge National Laboratory, U.S. Department of Energy, Oak Ridge, Tenn., USA, 2005.

Monnin, E., Indermühle, A., Dällenbach, A., Flückiger, J., Stauffer, B., Stocker, T. F., Raynaud, D., and Barnola, J.-M.: Atmospheric CO_2 concentrations over the last glacial termination, Science, 291, 112–114, 2001.

Mook, W. G.: ^{13}C in atmospheric CO_2, Netherlands J. Sea Res., 20, 211–223, 1986.

Munhoven, G.: Modelling glacial-interglacial atmospheric CO_2 variations: the role of continental weathering, Ph.D. thesis, Université de Liège, Liège, Belgium, 1997.

Pataki, D. E., Ehleringer, J. R., Flanagan, L. B., Yakir, D., Bowling, D. R., Still, C. J., Buchmann, N., Kaplan, J. O., and Berry, J. A.: The application and interpretation of Keeling plots in terrestrial carbon cycle research, Global Biogeochem. Cycles, 17, 1022, doi:10.1029/2001GB001850, 2003.

Petit, J. R., Jouzel, J., Raynaud, D., Barkov, N. I., Barnola, J.-M., Basile, I., Bender, M., Chappellaz, J., Davis, M., Delaygue, G., Delmotte, M., Kotlyakov, V. M., Legrand, M., Lipenkov, V. Y., Lorius, C., Pépin, L., Ritz, C., Saltzman, E., and Stievenard, M.: Climate and atmospheric history of the past 420,000 years from the Vostok ice core, Antarctica, Nature, 399, 429–436, 1999.

Plattner, G.-K., Joos, F., and Stocker, T. F.: Revision of the global carbon budget due to changing air-sea oxygen fluxes, Global Biogeochem. Cycles, 16, 1096, doi:10.1029/2001GB001746, 2002.

Sabine, C. L., Feely, R. A., Gruber, N., Key, R. M., Lee, K., Bullister, J. L., Wanninkhof, R., Wong, C. S., Wallace, D. W. R., Tilbrook, B., Millero, F. J., Peng, T.-H., Kozyr, A., Ono, T., and Rios, A. F.: The oceanic sink for anthropogenic CO_2, Science, 305, 367–371, 2004.

Scholze, M., Kaplan, J. O., Knorr, W., and Heimann, M.: Climate and interannual variability of the atmosphere-biosphere $^{13}CO_2$ flux, Geophys. Res. Lett., 30, 1097, doi:10.1029/2002GL015631, 2003.

Schwander, J. and Stauffer, B.: Age difference between polar ice and the air trapped in its bubbles, Nature, 311, 45–47, 1984.

Schwander, J., Jouzel, J., Hammer, C. U., Petit, J.-R., Udisti, R., and Wolff, E.: A tentative chronology for the EPICA Dome Concordia ice core, Geophys. Res. Lett., 28, 4243–4246, 2001.

Siegenthaler, U., Stocker, T. F., Monnin, E., Lüthi, D., Schwander, J., Stauffer, B., Raynaud, D., Barnola, J.-M., Fischer, H., Masson-Delmotte, V., and Jouzel, J.: Stable carbon cycle-climate relationship during the late Pleistocene, Science, 310, 1313–1317, doi:10.1126/science.1120130, 2005.

Smith, H. J., Fischer, H., Wahlen, M., Mastroianni, D., and Deck, B.: Dual modes of the carbon cycle since the Last Glacial Maximum, Nature, 400, 248–250, 1999.

Steig, E. J., Brook, E. J., White, J. W. C., Sucher, C. M., Bender, M. L., Lehman, S. J., Morse, D. L., Waddington, E. D., and Clow, G. D.: Synchronous climate change in Antarctica and North Atlantic, Science, 282, 92–95, 1998a.

Steig, E. J., Morse, D. L., Waddington, E. D., and Polissar, P. J.: Using the sunspot cycle to date ice cores, Geophys. Res. Lett., 25, 163–166, 1998b.

Sturm, P., Leuenberger, M., and Schmidt, M.: Atmospheric O_2, CO_2 and $\delta^{13}C$ observations from the remote sites Jungfraujoch, Switzerland, and Puy de Dôme, France, Geophys. Res. Lett., 32, L17 811, doi:10.1029/2005GL023304, 2005.

Trudinger, C. M., Enting, I. G., Francey, R. J., Etheridge, D. M., and Rayner, P. J.: Long-term variability in the global carbon cycle inferred from a high-precision CO_2 and $\delta^{13}C$ ice-core record, Tellus, 51B, 233–248, 1999.

Volk, T. and Hoffert, M. I.: Ocean carbon pumps: analysis of relative strengths and efficiencies in ocean-driven atmospheric CO_2 changes, in: The carbon cycle and atmospheric CO_2: Natural variations archean and present, edited by: Sundquist, E. T. and Broecker, W. S., Geophys. Monograph, 32, 99–110, American Geophysical Union, Washington, D.C., USA, 1985.

Wolff, E. W., Kull, C., Chappellaz, J., Fischer, H., Miller, H., Stocker, T. F., Watson, A. J., Flower, B., Joos, F., Köhler, P., Matsumoto, K., Monnin, E., Mudelsee, M., Paillard, D., and Shackleton, N.: Modeling past atmospheric CO_2: results of a challenge, EOS, 86(38), 341, 345, 2005.

Yakir, D. and Sternberg, L. D. S. L.: The use of stabile isotopes to study ecosystem gas exchange, Oecologia, 123, 297–311, 2000.

Zeebe, R. E. and Wolf-Gladrow, D. A.: CO_2 in Seawater: Equilibrium, Kinetics, Isotopes, Elsevier Oceanography Book Series, vol. 65, Elsevier Science Publishing, Amsterdam, The Netherlands, 2001.